Dynamics and Control of a Deformable Gyrostat, Utilizing Continuum Vehicle Modes

Hari B. Hablani*
Rockwell International, Seal Beach, California

The paper deals with dynamics of a specific gyroscopic flexible spacecraft and with synthesis of its controller. The infinite number of associated gyroscopic modes are shown to have alternately a precession parallel and antiparallel to the stored momentum. Dependence of mode shapes on the rotor's momentum is investigated. Identities based on the vehicle's momentum and inertia considerations are devised. The stochastic response analysis of the spacecraft subject to arbitrary excitation permits a "modal cost analysis" of the vehicle. These developments show that, as rotor's momentum escalates, a larger number of modes are required to construct a truncated model having a prespecified accuracy. A controller is designed on the basis of the "minimum error excitation" approach, which is found to be almost as effective as an optimal state feedback controller. The destabilizing influence of the truncated modes is exposed by utilizing the robustness inequalities available in the literature.

Nomenclature

A_e, A_r, A = moments of inertia of $\mathcal{E}$ and $\mathcal{R}$, respectively, about the axis $0x$ or $0y$; $A = A_r + A_e$
$\tilde{A}_r$ = $A_r/m_e\ell^2$
a, ℓ = radius of the hub $\mathcal{R}$ and the length of each appendage
$\mathcal{E}$ = elastic appendages of the gyrostat
EI, ρ_b, m_e = bending rigidity and the mass per unit length of the appendage; $m_e = 2\rho_b\ell$
G'_{mLa}, G_{mLa} = $G_{mL}(z)$ and $dG_{mL}(z)/dz$, respectively, at $z=a$
$\tilde{G}'_{mLa}$ = $m_e^{1/2}\ell G'_{mLa}$
h = angular momentum of the rotor along the axis $0z$
$\tilde{h}$ = $h/(2\ell m_e EI)^{1/2}$
$\mathcal{N}(0,\cdot)$ = white noise with zero mean and intensity $(\cdot)$
$\mathcal{R}$ = rigid hub of the gyrostat
$u(x,t), v(x,t)$ = deformation of $\mathcal{E}$ along the axis $0x$ and $0y$, respectively
x,y,z = principal coordinate frame of the gyrostat
$\tilde{\omega}$ = $(m_e\ell^3/2EI)^{1/2}\omega$
Σ = $\sum_{m=1}^{\infty}$ or $\sum_{\gamma=1}^{\infty}$, depending on the context

Subscripts and Superscripts

a = corresponding function evaluated at $z=a$
$\bar{(\ )}$ = complex conjugate except in $\bar{\sigma}$
$\tilde{(\ )}$ = nondimensional quantity
$(\ )'$ = d/dz
$\dot{(\ )}$ = d/dt

I. Introduction

OVER the last decade, Meirovitch and his co-workers have devoted considerable attention to analysis of the dynamics of flexible gyroscopic spacecraft and synthesis of their controllers (see Refs. 1 and 2, for instance). Specifically, from a controls standpoint, they have advanced a theory on an "independent modal space controller" in which each mode is controlled independently. Instability due to control and observation spillover into the modeled uncontrolled modes is shown to be absent. The order of the mathematical model is suggested to be sufficiently high so that the truncation effects and modeling uncertainties are minimal. However, no attempt is made either to quantify these errors or to examine their influence on the controller. On the other hand, Skelton[3] has presented a theory on adaptive orthogonal filters which explicitly estimate not only the reduced model state vector but also modeling errors from various sources. In Ref. 4, Skelton introduced the concept of "modal cost analysis" leading to a *model error index,* which is a measure of the accuracy of the retained model. More recently, Sezer and Siljak[5] have advanced a procedure to validate reduced order models by determining the associated *suboptimality index,* which is shown to be related to the model error index of Skelton.[4] Control systems have been designed based on order reduction schemes of Refs. 4 and 5, but such applications are limited to nongyroscopic spacecraft; deformable gyroscopic space vehicles have never been analyzed in this way. This provides the motivation for the present paper. Although the paper considers a specific deformable gyrostat, the procedure is applicable to any gyroscopic spacecraft.

The gyrostat under examination is shown in Fig. 1. The vehicle modes of this spacecraft, called *gyroscopic modes* hereafter, are determined in Ref. 6 by a continuum approach, in contrast with the discrete approach in the works of Meirovitch and his associates. Section II shows that the gyroscopic modes have alternately a precession parallel and antiparallel to the wheel's momentum. Also, certain momentum and inertial identities are deduced in this section. In Sec. III, "modal cost analysis" is extended to the gyrostat in hand by analyzing its wide-sense stationary random vibrations in the presence of disturbances having various types of power spectral densities. Section IV offers yet another approach to facilitate truncation of the modes by representing deleted modes as a multiplicative perturbation in the input-output transfer function. Blending the techniques of order reduction formulated in these three sections we construct a reduced order model of a determinable accuracy in Sec. V. In Sec. VI, a full state optimal feedback regulator is compared with a suboptimal output feedback controller based on the "minimum error excitation" approach advanced by Kosut.[7] Influence of deleted modes on performance and stability of the output feedback controller is investigated in

Presented as Paper 82-1613 at the AIAA Guidance and Control Conference, San Diego, Calif., Aug. 9-11, 1982; submitted Oct. 25, 1982; revision received March 14, 1983.

*Member of Technical Staff; formerly NRC/NASA Research Associate, NASA Johnson Space Center. Member AIAA.

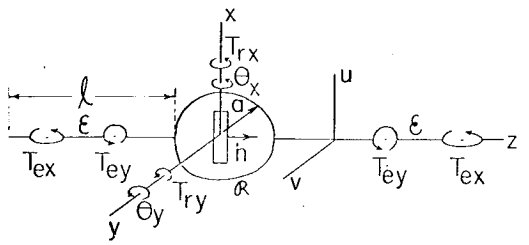

Fig. 1 A flexible gyroscopic spacecraft.

Sec. VII, where robustness inequalities by Sandell[8] are utilized. Section VIII presents numerical results which illustrate various aspects of the theory propounded in the previous sections. Our findings are summarized in Sec. IX. For numerical purposes the spacecraft is chosen to have the following parameters:

$$\ell = 100.0\ \text{m}, \qquad EI = 6.5\ \text{Nm},^2 \qquad \rho_b = 0.0215\ \text{kg/m}$$

$$\tilde{A}_r = 0.0005, \qquad a/\ell = 0.02 \tag{1}$$

The small value of A_r will allow an intense interaction between $\mathfrak{R}$, $\mathcal{E}$ and the wheel. The lowest frequency of the spacecraft with the parameters in Eq. (1) and $h = 0.0$ is 0.0255935 rad/s.

II. Modal Characteristics of a Gyroscopic Spacecraft

A. The Eigenvalue Problem

An antisymmetric gyroscopic mode $G_{mL}(z)$, $m = 1,\ldots,\infty$, of the spacecraft in Fig. 1 is governed by the following eigenvalue problem[6]:

$$EIG'''_{mL}(z) = \rho_b \omega_m^2 G_{mL}(z) \qquad a < z < \ell + a \tag{2}$$

$$G_{mLa} = aG'_{mLa}$$

$$2EI(aG'''_{mLa} - G''_{mLa}) = (-\omega_m h + \omega_m^2 A_r) G'_{mLa} \qquad z = a$$

$$G''_{mL} = G'''_{mL} = 0 \qquad z = \ell + a \tag{3}$$

where $G_{mL}(z)$ is a *real* function. It obeys the familiar beam equation, but the boundary condition at $z = a$ involves the modal frequency ω_m linearly as well as quadratically and the rotor's momentum h. Throughout the paper the range of m will be $1,\ldots,\infty$, unless specified otherwise. The orthonormality obeyed by $G_{mL}(z)$ is[6]

$$\int [EIG'_{mL}(z) G''_{nL}(z)/\omega_m\omega_n + \rho_b G_{mL}(z) G_{nL}(z)]\,dz + A_r G'_{mLa} G'_{nLa} = \delta_{mn} \tag{4}$$

where δ_{mn} is the Kronecker delta.

With the above preliminaries Eqs. (2) and (3) can be shown to have the following solution:

$$G_{mL}(z') = (G'_{mLa}/2\sigma_m)[(1-\beta_m)\sinh\sigma_m z' + (1+\beta_m)\sin\sigma_m z' + (\gamma_m + a\sigma_m)\cosh\sigma_m z' - (\gamma_m - a\sigma_m)\cos\sigma_m z'] \tag{5}$$

where $z' = z - a$ and

$$\beta_m \triangleq \frac{h_m(ch+c) + 2\epsilon_m}{\delta_m} \qquad \gamma_m \triangleq \frac{h_m(sh+s) - 2a\sigma_m\epsilon_m}{\delta_m}$$

$$\epsilon_m \triangleq a\sigma_m(ch-c) + (sh-s)$$

$$\delta_m \triangleq 2\{a\sigma_m(ch+c) + (sh+s)\}$$

$$h_m \triangleq \frac{\pm h\sigma_m}{\sqrt{EI\rho_b}} - \frac{A_r\sigma_m^3}{\rho_b}$$

$$sh \triangleq \sinh\sigma_m\ell \qquad ch \triangleq \cosh\sigma_m\ell \qquad s \triangleq \sin\sigma_m\ell \qquad c \triangleq \cos\sigma_m\ell \tag{6}$$

The σ_m, always positive, is the solution of the frequency equation

$$(s\cdot ch - c\cdot sh) + a\sigma_m[a\sigma_m(c\cdot sh + s\cdot ch) + 2s\cdot sh] + (\tilde{A}_r\sigma_m^2\ell^2 \mp \tilde{h})\sigma_m\ell(1 + c\cdot ch) = 0 \tag{7}$$

Note the double signs in h_m and $\tilde{h}$ in Eqs. (6) and (7). It turns out that the modal frequencies ω_m are related to σ_m as

$$\omega_m \triangleq (EI/\rho_b)^{1/2}\sigma_m^2 \qquad m = 1,3,5,\ldots$$

$$\triangleq -(EI/\rho_b)^{1/2}\sigma_m^2 \qquad m = 2,4,6,\ldots \tag{8}$$

where the odd and the even numbered modes are furnished respectively by the upper and the lower sign of h in Eq. (7). Similarly, the odd and the even numbered $G_{mL}(z')$ in Eq. (5) will respectively take the upper and the lower sign in h_m. It is not self-evident that the signs of ω_m are as claimed by Eq. (8). However, Eq. (8) is numerically verified by the following *momentum identities* produced by the phase space modal analysis[6]

$$h\Sigma G'^2_{mLa}/\omega_m = 1 \qquad h\Sigma G'_{mLa}G'_{mLe}/\omega_m = 1 \tag{9}$$

where G'_{mLe} is the slope of $G_{mL}(z)$ at the location of $T_e(t)$. The two identities respectively correspond to T_r and T_e, where

$$T_r \triangleq T_{rx} + iT_{ry} \qquad T_e \triangleq T_{ex} + iT_{ey} \qquad i \triangleq \sqrt{-1} \tag{10}$$

As shown in Fig. 1 the torques T_r and T_e act symmetrically on the spacecraft. Also, it is found that, for a sufficiently small value of h, the frequency ω_1 is close to the precessional frequency $\omega_p = h/A$ obtained by treating the appendages as rigid. This leads us to conclude that the odd and the even numbered modes have, respectively, precession parallel and antiparallel to the rotor's momentum. As such, the two sets of modes in Eq. (8) will be respectively called *precessional* and *antiprecessional* modes.

The slope G'_{mLa} in the mode shape $G_{mL}(z)$ [Eq. (5)] is determined by applying the normality condition, Eq. (4), for $m = n$. Substitution of $G_{mL}(z)$ and its derivatives in Eq. (4), integration, and extensive algebra yield

$$G'^2_{mLa}[(\sqrt{EI\rho_b}/\omega_m)\{[(1-\beta_m)^2 + (\gamma_m + a\sigma_m)^2]\sinh 2\sigma_m\ell/4\sigma_m + (1-\beta_m)(\gamma_m + a\sigma_m)\cosh 2\sigma_m\ell/2\sigma_m + (1+\beta_m)(\gamma_m - a\sigma_m)\cos 2\sigma_m\ell/2\sigma_m + [(\gamma_m - a\sigma_m)^2 - (1+\beta_m)^2]\sin 2\sigma_m\ell/4\sigma_m + (2\beta_m + \gamma_m^2 + a^2\sigma_m^2)\ell + (\beta_m a\sigma_m - \gamma_m)/\sigma_m\} + A_r] = 1 \tag{11}$$

The gyroscopic mode $G_{mL}(z)$ is thus completely determined. The above modal characteristics will be numerically illustrated and discussed in Sec. VIII. A.

The momentum identities, Eq. (9), can be used to determine accuracy of any truncated model from the standpoint of the vehicle's angular momentum. We now turn our attention to the identities which can be obtained from inertia considerations.

B. Inertial Modal Identities

These identities are constructed by comparing two transfer functions of the spacecraft obtained by using the gyroscopic modes, as defined here, and the appendage modes which are ordinarily used. The basic procedure is inherited from Hughes.[9] We proceed as follows.

Utilizing the modal analysis of Ref. 6, the following relation between the attitude $\theta(s) \triangleq \theta_x(s) + i\theta_y(s)$, where s is the Laplace variable, of the spacecraft in Fig. 1 and the torques $T_r(s)$ and $T_e(s)$ can be derived. We ignore the distinction between a time-dependent quantity and its Laplace transform. For convenience, the argument s, when not necessary, will be ignored. The transfer function relation is

$$s^2\theta = \left[\frac{s}{s-i\omega_p} - \sum \frac{s^2 g_m G'_{mLa}}{(s-i\omega_m)(s-i\omega_p)}\right]\frac{T_r}{A} + \left[\frac{s}{s-i\omega_p} - \sum \frac{s^2 g_m G'_{mLe}}{(s-i\omega_m)(s-i\omega_{pe})}\right]\frac{2T_e}{A} \tag{12}$$

where

$$g_m \triangleq \int z G_{ma}(z)\,dm \qquad G_{ma}(z) \triangleq G_{mL}(z) - zG'_{mLa} \tag{13}$$

and dm is an element of mass. The function $G_{ma}(z)$ is a partial vehicle mode and represents the deformation of the appendage during the mode m. The coefficient g_m embodies the integrated influence of the appendage deformation on the attitude of the rigid body. For its evaluation, the entire mode shape $G_{mL}(z)$ is not required. This is proved by recognizing that the angular momentum residing in a gyroscopic mode is zero[6]; mathematically, we have

$$\int z G_{mL}(z)\,dm + (A_r - h/\omega_m) G'_{mLa} = 0 \tag{14}$$

With the aid of Eq. (14), Eq. (13) transforms to

$$g_m = -(A - h/\omega_m) G'_{mLa} = -A(1 - \omega_p/\omega_m) G'_{mLa} \tag{15}$$

In line with the terminology in Ref. 9, the g_m may be called a *modal momentum coefficient*.

We now obtain a transfer function similar to Eq. (12) by using the cantilever modes $F_\gamma(z)$, $\gamma = 1,\ldots,\infty$, of the appendages $\mathcal{E}$ of the spacecraft in Fig. 1. Let Ω_γ and f_γ be, respectively, the frequency and a modal momentum coefficient associated with the mode $F_\gamma(z)$. The coefficient f_γ is akin to g_m and has the following properties[9]:

$$f_\gamma \triangleq \int z F_\gamma(z)\,dm \qquad \Sigma f_\gamma^2 = A_e \tag{16}$$

Note that there does not exist any simple relation between the mode $F_\gamma(z)$ and the partial vehicle mode $G_{ma}(z)$. It is straightforward to derive the following transfer function similar to Eq. (12):

$$s^2\theta = \left\{\frac{s-i\omega_p}{s} - \sum \frac{s_\gamma f_\gamma^2}{A}\right\}^{-1}\left\{\frac{T_r}{A} + [1 - \Sigma s_\gamma f_\gamma F'_\gamma(z_e)]\frac{2T_e}{A}\right\} \tag{17}$$

where $s_\gamma = s^2/(s^2+\Omega_\gamma^2)$.

Since the transfer functions (12) and (17) are for the same spacecraft, we equate the coefficients of T_r, determine

$$\lim_{s\to\infty}$$

and utilize the second part of Eq. (16). There follows

$$A/A_r = 1 - \Sigma g_m G'_{mLa} \tag{18}$$

Implication of the identity (18) is that the infinite sum in the right side is proportional to the moment of inertia A_e. A comparison of the coefficients of $2T_e$ in Eqs. (12) and (17) leads to

$$(A/A_r)[1 - \Sigma f_\gamma F'_\gamma(z_e)] = 1 - \Sigma g_m G'_{mLe} \tag{19}$$

Two more identities can be discovered as follows. At $s = i\omega_m$, the coefficient of T_r in Eq. (12) is unbounded (because natural damping of the appendage is not yet included in the analysis), which means that the inverse of the coefficient must be zero. There follows one identity

$$\frac{\omega_m - \omega_p}{\omega_m} - \sum\left\{\frac{\omega_m^2}{\omega_m^2 - \Omega_\gamma^2}\right\}\frac{f_\gamma^2}{A} = 0 \tag{20}$$

If we replace ω_m^2 in the numerator of the quantity within braces by $(\omega_m^2 - \Omega_\gamma^2 + \Omega_\gamma^2)$, minor manipulations with the aid of Eq. (16) lead to the second identity

$$\Sigma[\Omega_\gamma^2/(\Omega_\gamma^2 - \omega_m^2)] f_\gamma^2 = (h - A_r\omega_m)/\omega_m \tag{21}$$

We next recognize that at $s = i\Omega_\gamma$ the coefficient of T_r in Eq. (17) is zero. Consequently, the substitution of $s = i\Omega_\gamma$ in the coefficient of T_r in Eq. (12) furnishes the following identity:

$$\Omega_\gamma \Sigma A G'^2_{mLa}(\omega_m - \omega_p)/\omega_m(\omega_m - \Omega_\gamma) = 1 \tag{22}$$

While deriving Eq. (22), it is assumed that $\Omega_\gamma \neq \omega_p$.

Some of the identities (18-22) will be numerically verified in Sec. VIII.B. These identities, along with the momentum identities (9), will be used in Sec. VIII.E as metrics to measure the accuracy of the truncated model. The identities serve the stated purpose in the early stages of dynamic modeling, when nothing is known about the control objective of the spacecraft or about the disturbances it will encounter. However, as these quantities along with the sensed variables and input quantities become known, the above metrics should be supplemented with the modal cost analysis to which we now devote our attention.

III. Modal Cost Analysis: A Frequency Domain Approach

The modal cost analysis, as devised by Skelton and Hughes,[10] is restricted to nongyroscopic spacecraft subject to white noise disturbances for which they applied a time domain approach. In Ref. 11, the technique is diversified to include nonwhite disturbances via frequency domain. The objective of this section is to extend the modal cost analysis further by applying it to the gyroscopic spacecraft in Fig. 1. We will derive literal modal cost expressions for attitude, attitude rate, and "energy" control under disturbances having arbitrary power spectral density. For this purpose the residue calculus of complex variable theory will be used. In the following analysis the cross-correlation between two different modes has been ignored. This is justified because the modal overlap ratio

$$r = 2\zeta_m|\omega_m|/(|\omega_m| - |\omega_{m-1}|) \tag{23}$$

for $h = 0.0$, $\zeta_m = 0.005$, and $A_r = 0.0$ is found to be 0.01446 and 0.30377 for $m = 2$ and 60, respectively. Although $r \ll 1$ for structures such as beams employed here, it can be >1 for structures having tightly clustered frequencies. For example, for a certain shell structure the r was found to be 5.984 and 1.387 for $m = 2$ and $m = 3$ (Ref. 12). The modal damping coefficient ζ_m is discussed after Eq. (33). In addition to the above assumption, we also ignore the cross-correlation between the vehicle's angular momentum

$$H(t) = H_x(t) + iH_y(t) \tag{24}$$

and the modal coordinate $\alpha_m(t)$ associated with the eigenvalue problem (2). In the early phase of our research we did incorporate this cross-correlation; however, subsequent

numerical experience showed that it is negligible as compared to the modal autocorrelation.

We now intend to determine the variance $\hat{\alpha}_m$ of the modal coordinate $\alpha_m(t)$, where

$$\hat{\alpha}_m = \lim_{t\to\infty} E(\bar{\alpha}_m \alpha_m) \tag{25}$$

But before its determination we will review a few commonly confronted control objectives. For example, let the performance objective be to control the "energy" of the spacecraft; that is,

$$J_E = \lim_{t\to\infty} E\int [EI(u''^2+v''^2)+\rho_b\{(\dot{u}+z\dot{\theta}_y)^2 + (\dot{v}-z\dot{\theta}_x)^2\}]\,dz \tag{26}$$

where E is an expectation operator. The modal analysis of Ref. 6 reduces Eq. (26) to $J_E=\Sigma\hat{\alpha}_m$, which evidently involves $\hat{\alpha}_m$. Here, J_E is neither total energy nor Hamiltonian of the spacecraft.

The $\hat{\alpha}_m$ is also encountered when an attitude or an attitude rate controller are desired. Consider the attitude control first. Reference 6 furnishes the following modal expansion:

$$\theta(t)=iH(t)/h+\Sigma\theta_m(t) \qquad \theta_m(t)\triangleq G'_{mLa}\alpha_m(t)/\omega_m \tag{27}$$

With the aid of the assumptions mentioned before, we have

$$J_\theta \triangleq \lim_{t\to\infty} E(\bar{\theta}\theta) = \lim_{t\to\infty} E[\bar{H}H/h^2+\Sigma\bar{\theta}_m\theta_m] \tag{28}$$

However, by utilizing the definition of $\theta_m(t)$ from Eq. (27), the variance $\hat{\theta}_m$ can be related to the $\hat{\alpha}_m$ as follows:

$$\hat{\theta}_m = \lim_{t\to\infty} E[\bar{\theta}_m(t)\theta_m(t)] = G'^2_{mLa}\hat{\alpha}_m/\omega_m^2 \tag{29}$$

Similarly, for attitude rate control one has the following index:

$$J_{\dot{\theta}} \triangleq \lim_{t\to\infty} E(\dot{\bar{\theta}}\dot{\theta}) \tag{30}$$

where the attitude rate $\dot{\theta}$ has the following modal expansion[6]:

$$\dot{\theta}=i\Sigma\theta_{\dot{m}}(t) \qquad \theta_{\dot{m}}(t)\triangleq G'_{mLa}\alpha_m(t) \tag{31}$$

The expansion (31) and the assumption of negligible modal cross-correlation transform Eq. (30) to

$$J_{\dot{\theta}}=\Sigma\hat{\theta}_{\dot{m}} \qquad \hat{\theta}_{\dot{m}} \triangleq \lim_{t\to\infty} E(\bar{\theta}_{\dot{m}}\theta_{\dot{m}}) = G'^2_{mLa}\hat{\alpha}_m \tag{32}$$

Thus we see that the variance $\hat{\alpha}_m$ is present in most control objectives of interest. We now proceed to its determination.

The time dependence of the modal coordinate $\alpha_m(t)$ is[6]

$$\dot{\alpha}_m = (-\zeta_m|\omega_m|+i\omega_m)\alpha_m - iG'_{mLa}T_r \tag{33}$$

where, of course, the modal damping coefficient ζ_m has been added after modal analysis is completed. It represents light damping present naturally in most structures. Since the damping is light, the undamped modes $G_{mL}(z)$ are inconsequentially different from the damped natural modes. Also, we observe that although $\zeta_m\to 0$ it is not equal to zero. If $\zeta_m=0$, control induced instabilities exist and a reliable control system cannot be designed.[13] The absolute sign in $\zeta_m|\omega_m|$ is required because ω_m is negative for $m=2,4,\ldots$. In Eq. (33) only the disturbing torque T_r is modeled; the torque T_e acting on $\mathcal{E}$ will not be considered. The coefficient G'_{mLa} of T_r is an index of controllability or disturbability of the mode $\alpha_m(t)$ (Ref. 6).

The reader must have noticed that a control variable is not present in the performance indexes J_E, J_θ, and $J_{\dot{\theta}}$. This is because the modal cost analysis is an open loop response analysis. However, it is desirable to let actuator activity influence the mode selection process, because only in the presence of actuator activity can the worthiness of a model be tested.[14] Since a control policy for the present gyrostat is not yet designed, the only way of incorporating actuator dynamics is to treat the dynamics as a stochastic process to which white noise is an input. Consequently, let T_r be a second-order stochastic process governed by

$$\ddot{T}_r+2\zeta_a\omega_a\dot{T}_r+\omega_a^2T_r=\omega_a^2\nu_a \qquad \nu_a\triangleq\nu_{ax}+i\nu_{ay} \tag{34}$$

$$\nu_{ax}\triangleq\mathfrak{N}(0,V_{ax}) \qquad \nu_{ay}\triangleq\mathfrak{N}(0,V_{ay}) \qquad \nu_a\triangleq\mathfrak{N}(0,V_a)$$

$$V_a=V_{ax}+V_{ay} \tag{35}$$

where the white noises ν_{ax} and ν_{ay} are uncorrelated. Equations (34) and (35) furnish the following power spectral density of T_r (see Ref. 15, Ex. 1.11)

$$P_{Tr}(\omega)=V_a\omega_a^4/(-\omega^2+2i\omega\zeta_a\omega_a+\omega_a^2)(-\omega^2-2i\omega\zeta_a\omega_a+\omega_a^2) \tag{36}$$

Similarly, the power spectral density of α_m from Eq. (33) is

$$P_{\alpha m}(\omega)=P_{Tr}(\omega)G'^2_{mLa}/\{\zeta_m|\omega_m| + i(\omega-\omega_m)\}\{\zeta_m|\omega_m|-i(\omega-\omega_m)\} \tag{37}$$

We now invoke the theorem (Ref. 15, Theorem 1.50)

$$\hat{\alpha}_m=\int_{-\infty}^{\infty} P_{\alpha m}(\omega)\,d\omega/2\pi \tag{38}$$

and the following relation from the residue calculus[16]:

$$\int_{-\infty}^{\infty} f(\omega)\,d\omega = 2\pi i\sum_k \mathrm{Res}(a_k) \tag{39}$$

where $f(\omega)$ is an algebraic function of ω such that its denominator is of degree at least 2 greater than the numerator; $\mathrm{Res}(a_k)$ is the residue of $f(\omega)$ at the pole a_k. With the aid of Eqs. (38) and (39) and the fact that the structural damping coefficient ζ_m is close to zero, the following relation is obtained:

$$\hat{\alpha}_m = G'^2_{mLa}P_{Tr}(\omega_m)/2\zeta_m|\omega_m| \tag{40}$$

where $P_{Tr}(\omega_m)$ is the power spectral density of the actuator disturbance at the modal frequency ω_m.

Selection of a mode depends not only on internal disturbances such as those due to actuators, but also on external disturbances such as those due to meteorite impacts. For illustrative purposes, let there be a stochastic disturbance of first order, namely, an exponentially correlated noise ξ_e described by

$$\dot{\xi}_e=-\xi_e/\tau+\nu_e, \quad \nu_e=\mathfrak{N}(0,V_e) \tag{41}$$

where $\xi_e(t)$ replaces $T_r(t)$ in Eq. (33). Following the preceding line of argument, we can prove that

$$\hat{\alpha}_m = G'^2_{mLa}P_{\xi e}(\omega_m)/2\zeta_m|\omega_m| \tag{42}$$

where $P_{\xi e}(\omega_m)$ is the power spectral density of the ξ_e at the modal frequency ω_m. That is,

$$P_{\xi e}(\omega_m)=V_e\tau^2/(1+\omega_m^2\tau^2) \tag{43}$$

Comparison of the variances (40) and (42) lead to a plausible speculation that, for a disturbance having arbitrary power

spectral density $P(\omega)$, the variance $\hat{\alpha}_m$ will be

$$\hat{\alpha}_m = G'^2_{mLa} P(\omega_m)/2\zeta_m|\omega_m| \tag{44}$$

The variances (40), (42), and (44) will be illustrated in Sec. VIII.C.

Thus we have determined the variance $\hat{\omega}_m$ for the present spacecraft subject to nonwhite disturbances.

There exists some similarity between the process of order reduction by modal cost analysis and by singular value decomposition of a system having "balanced representation" developed by Moore.[17] For example, for attitude control the variance $\hat{\theta}_m$ in Eq. (29) involves product of controllability $[G'^2_{mLa}$ from Eq. (44)] and observability $[G'^2_{mLa}$ from Eq. (29)]. On the other hand, in Moore's procedure one finds singular values of the controllability and observability Grammians of a balanced system and retains the most controllable and the most observable part of the system. It is, however, not clear whether the modes selected by any open loop order reduction scheme will remain the most significant ones in the closed loop system. A question of a different nature also arises, that is, how to characterize deleted modes so that their influence on bandwidth of a multivariable controller designed on the basis of a reduced order model can be studied. The next section offers an answer to this question.

IV. Deleted Modes as Modeling Uncertainties: A Frequency Domain Approach

Omitted dynamics can be expressed as an additive or a multiplicative perturbation in the idealized transfer function of the system. Since the multiplicative representation does not require knowledge of controller gains, it is useful even when analyzing an open loop situation. Therefore, in this section, the deleted modes will be expressed as a multiplicative perturbation. In Secs. VII and VIII.G, examples of an additive perturbation will be seen.

Construction of a transfer function requires knowledge of input and output variables. Let the spacecraft be equipped with only two torquers, T_{rx} and T_{ry}, and with four sensors measuring θ_x, $\dot{\theta}_x$, θ_y, and $\dot{\theta}_y$. In this section we assume that the torquers and the sensors are idealized. Thus we have the following input vector $\boldsymbol{u}(t)$, the output vector $\boldsymbol{z}(t)$, and a relationship between the two:

$$\boldsymbol{u}(t) \triangleq [T_{rx}\, T_{ry}]^T \qquad \boldsymbol{z} \triangleq [\theta_x \theta_y \dot{\theta}_x \dot{\theta}_y]^T \qquad \boldsymbol{z} = \boldsymbol{G}\boldsymbol{u} \tag{45}$$

The transfer function matrix $\boldsymbol{G}$ involves all the infinite modes. It can be split such that

$$\boldsymbol{G} \triangleq \boldsymbol{G}_E + \boldsymbol{G}_H \tag{46}$$

where $\boldsymbol{G}_E$ and $\boldsymbol{G}_H$ respectively contain the retained and the deleted modes. Equation (46) can be rearranged as

$$\boldsymbol{G} \triangleq (\boldsymbol{I} + \boldsymbol{G}_H \boldsymbol{G}_E^{\dagger})\boldsymbol{G}_E, \qquad \boldsymbol{G}_E^{\dagger} = (\boldsymbol{G}_E^* \boldsymbol{G}_E)^{-1} \boldsymbol{G}_E^* \tag{47}$$

where $\boldsymbol{G}_E^{\dagger}$ is a left pseudoinverse. The superscript * denotes conjugate transpose. $\boldsymbol{I}$ in Eq. (47) is an identity matrix of size 4×4. The arrangement (47) implies that the uncertainty $\boldsymbol{G}_H \boldsymbol{G}_E^{\dagger}$ is at the output of the model. The right pseudoinverse cannot be used in the present circumstances, because it involves inversion of a singular 4×4 matrix $\boldsymbol{G}_E \boldsymbol{G}_E^*$ unlike the inversion of a complex 2×2 matrix $\boldsymbol{G}_E^* \boldsymbol{G}_E$ in the left pseudoinverse defined in Eq. (47). Let

$$\boldsymbol{L}(i\omega) \triangleq \boldsymbol{G}_H(i\omega)\boldsymbol{G}_E^{\dagger}(i\omega) \tag{48}$$

Thus $\boldsymbol{L}(i\omega)$ is a multiplicative perturbation in the idealized transfer function $\boldsymbol{G}_E(i\omega)$. The following is an example of a scalar norm of the perturbation matrix $\boldsymbol{L}$ in Eq. (48):

$$\bar{\sigma}(\boldsymbol{L}) \triangleq \lambda_{mx}^{1/2}(\boldsymbol{L}^*\boldsymbol{L}) \tag{49}$$

where $\bar{\sigma}(\cdot)$ is the maximum singular value of $(\cdot)$, and $\lambda_{mx}(\cdot)$ is the maximum eigenvalue of $(\cdot)$. We have introduced this example because it will be useful in Sec. VII.

There exist basic differences between a nongyroscopic and a gyroscopic spacecraft. In the former case, a vehicle mode is governed by a second-order equation, the attitude angles θ_x and θ_y are uncoupled, and the rigid modes have zero frequency. In the latter case, a gyroscopic mode is described by two coupled first-order equations, the angles θ_x and θ_y are coupled, and the zero-frequency rigid modes are replaced by the first precessional mode having frequency ω_1. Because of these differences, construction of $\boldsymbol{L}$ for the two types of spacecraft is accomplished separately as follows.

A modal analysis of the spacecraft in Fig. 1 for $h=0.0$ is straightforward.[6] Omitting the details, it can be shown that $\boldsymbol{G}(s)$ in Eq. (45) is

$$\boldsymbol{G}(s) \triangleq \begin{bmatrix} 1/As^2 + \Sigma a_m & 0 \\ 0 & 1/As^2 + \Sigma a_m \\ 1/As + \Sigma s a_m & 0 \\ 0 & 1/As + \Sigma s a_m \end{bmatrix}$$

$$a_m \triangleq \frac{w'^2_{ma}}{s^2 + 2s\zeta_m\omega_m + \omega_m^2} \tag{50}$$

where w'_{ma} is the slope of the mth mode at $z=a$. Whatever may be the policy of selecting the modes, let $m=1,\ldots,N$ be the modes retained in $\boldsymbol{G}_E$. The modes $N+1,\ldots,\infty$ are included in $\boldsymbol{G}_H$. By carrying out the operations in Eqs. (47) and (48), the reader can show that

$$\boldsymbol{L}^*\boldsymbol{L} = [d_H/(1+\omega^2)d_E]\boldsymbol{E} \tag{51}$$

where

$$d_E \triangleq \left\{-1/A\omega^2 + \sum_{m=1}^{N}(-\omega^2+\omega_m^2)d_m\right\}^2 + \left\{\sum_{m=1}^{N} 2\omega\zeta_m\omega_m d_m\right\}^2$$

$$d_H \triangleq \left\{\sum_{m=N+1}^{\infty}(-\omega^2+\omega_m^2)d_m\right\}^2 + \left\{\sum_{m=N+1}^{\infty} 2\omega\zeta_m\omega_m d_m\right\}^2$$

$$d_m \triangleq w'^2_{ma}/\{(-\omega^2+\omega_m^2)^2 + (2\omega\zeta_m\omega_m)^2\}$$

$$\boldsymbol{E} \triangleq \begin{bmatrix} 1 & 0 & -i\omega & 0 \\ 0 & 1 & 0 & -i\omega \\ i\omega & 0 & \omega^2 & 0 \\ 0 & i\omega & 0 & \omega^2 \end{bmatrix} \tag{52}$$

The eigenvalues of the Hermitian matrix $\boldsymbol{E}$ are 0, $(1+\omega^2)$ with multiplicity 2. Consequently, the $\bar{\sigma}$ is

$$\bar{\sigma}(\boldsymbol{L}) = (d_H/d_E)^{1/2} \tag{53}$$

To consider gyroscopic situations, we express the complex modal expansions (27), (31), and the modal equation (33) in a real form. Also, the angular momentum equations

$$\dot{H}_x = T_{rx} \qquad \dot{H}_y = T_{ry} \tag{54}$$

are utilized to eliminate $H(t)$ from Eq. (27). Laplace transformation and algebraic manipulations lead to

$$G(s) \triangleq \begin{bmatrix} \Sigma e_m & -1/hs + \Sigma s e_m/\omega_m \\ 1/hs - \Sigma s e_m/\omega_m & \Sigma e_m \\ \Sigma s e_m & -\Sigma \omega_m e_m \\ \Sigma \omega_m e_m & \Sigma s e_m \end{bmatrix}$$

$$e_m(s) = \frac{G'^{22}_{mLa}}{s^2 + 2s\zeta_m|\omega_m| + \omega_m^2} \tag{55}$$

which may be compared with Eq. (50). Since $G(s)$ in Eq. (55) is full, a literal evaluation of $\bar{\sigma}$ which was done for $h=0.0$ is not possible here.

Thus the formulation for expressing deleted modes as a multiplicative perturbation in the idealized transfer function is complete and will be illustrated in Sec. VIII.

V. Construction of a Finite Model

So far we have probed the process of model truncation of a gyroscopic spacecraft from three viewpoints: the momentum and the inertial modal identities, the modal cost analysis, and the deleted modes as a multiplicative perturbation. In Sec. VIII.E, these three viewpoints will be blended so as to construct a finite model, for which the accuracy can be determined, of the spacecraft in Fig. 1.

Let S be the set of retained modes $m_1, m_2, \ldots, m_N$; that is,

$$S \triangleq (m_1, m_2, \ldots, m_N) \tag{56}$$

Then the real mathematical model of dynamics of the gyrostat in hand will appear as follows. The internal disturbance due to the actuators (34) and (35) will be ignored, but the exponentially correlated external disturbance (41) will be considered. The model is

a) angular momentum equations:

$$\dot{H}_x = T_{rx} + \xi_x, \quad \dot{H}_y = T_{ry} + \xi_y \tag{57a}$$

b) retained modal equations:

$$\dot{\alpha}_{mR} = -\zeta_m|\omega_m|\alpha_{mR} - \omega_m\alpha_{mI} + G'_{mLa}(T_{ry} + \xi_y)$$

$$\dot{\alpha}_{mI} = -\zeta_m|\omega_m|\alpha_{mI} + \omega_m\alpha_{mR} - G'_{mLa}(T_{rx} + \xi_x) \tag{57b}$$

where $\alpha_m(t) \triangleq \alpha_{mR}(t) + i\alpha_{mI}(t)$, $m \in S$; c) disturbance dynamics, Eq. (41):

$$\dot{\xi}_x = -\xi_x/\tau + \nu_x \qquad \nu_x = \mathfrak{N}(0, V_x)$$

$$\dot{\xi}_y = -\xi_y/\tau + \nu_y \qquad \nu_y = \mathfrak{N}(0, V_y) \tag{57c}$$

d) actuator dynamics, Eq. (34):

$$\ddot{T}_{rx} + 2\zeta_a\omega_a\dot{T}_{rx} + \omega_a^2 T_{rx} = \omega_a^2 u_x(t)$$

$$\ddot{T}_{ry} + 2\zeta_a\omega_a\dot{T}_{ry} + \omega_a^2 T_{ry} = \omega_a^2 u_y(t) \tag{57d}$$

One of the saliencies of the above model is that it includes angular momentum equations. The mathematical models of gyroscopic spacecraft available in the literature have not been so constructed. See Meirovitch,[1] Oz and Meirovitch,[2] Hughes and Skelton,[18] Likins and Ohkami,[19] and Juang and Balas.[20] The reason for our doing so is the modal expansion (27).

The state space model corresponding to Eqs. (57) is

$$\dot{\boldsymbol{x}}(t) = \boldsymbol{A}\boldsymbol{x}(t) + \boldsymbol{B}\boldsymbol{u}(t) + \boldsymbol{D}\boldsymbol{\nu}(t), \quad \boldsymbol{\nu}(t) \triangleq \mathfrak{N}(0, \boldsymbol{V}) \tag{58}$$

where the control vector $\boldsymbol{u}$ and the disturbance vector $\boldsymbol{\nu}$ are defined as

$$\boldsymbol{u}(t) \triangleq [u_x(t) \quad u_y(t)]^T \qquad \boldsymbol{\nu}(t) \triangleq [\nu_x(t) \quad \nu_y(t)]^T \tag{59}$$

The $\boldsymbol{u}$ in Eq. (45) was defined by ignoring the actuator dynamics; we have not done so in Eqs. (57-59). The state vector $\boldsymbol{x}(t)$ is

$$\boldsymbol{x}(t) = [H_x, H_y, \alpha_{m_1R}, \alpha_{m_1I} \ldots, \alpha_{m_NR}, \alpha_{m_NI}, \xi_x, \xi_y, T_{rx}, t_x, T_{ry}, t_y]$$

where

$$t_{x,y}(t) \triangleq (\dot{T}_{rx,y} + \zeta_a\omega_a T_{rx,y})/\omega_{ad} \qquad \omega_{ad} \triangleq \omega_a(1-\zeta_a^2)^{1/2}$$

To conserve space the matrices $\boldsymbol{A}$, $\boldsymbol{B}$, and $\boldsymbol{D}$ will not be detailed here. The measurement vector $\boldsymbol{z}$ in Eq. (45) is related to $\boldsymbol{x}$ as

$$\boldsymbol{z} = \boldsymbol{C}\boldsymbol{x} \tag{60}$$

With the aid of the expansions (27) and (31), it is easy to construct the matrix $\boldsymbol{C}$. We continue to assume that the sensors are perfect.

The modes $m_1, \ldots, m_N$ and the numeral counterpart of the finite model (57) will be given in Sec. VIII.E.

VI. Design of a Suboptimal Output Feedback Controller

In Sec. VIII.E, the state vector $\boldsymbol{x}$ will be chosen to have the size 42×1 and it will contain $N=17$ gyroscopic modes. Accuracy of this model is also determined in Sec. VIII.E. Ashkenazi and Bryson[21] show that a Kalman filter is undesirable when there are large modeling uncertainties. We assume that such a situation prevails here. Moreover, the "independent modal space control" by Oz and Meirovitch[2] requires as many actuators as the number of controlled modes, a condition not satisfied presently. On the other hand, Ref. 11 shows that, for a nongyroscopic spacecraft, a suboptimal output feedback controller based on the minimum error excitation (MEE) approach, advanced by Kosut,[7] performs nearly as well as an optimal state feedback (OSFB) does. Therefore, in this paper, a controller will be designed via the MEE approach.

The performance objective for which the modes will be selected in Sec. VIII.E is attitude and attitude rate control; that is,

$$J = \lim_{t\to\infty} E[\theta_x^2(t) + \theta_y^2(t) + \beta\{\dot{\theta}_x^2(t) + \dot{\theta}_y^2(t)\} + \rho\{u_x^2(t) + u_y^2(t)\}] \tag{61}$$

Evidently, the controlled variables are the same as the measured variables $\boldsymbol{z}$. Regarding the weighting scalar β, in Sec. VIII.F we will arbitrarily choose

$$\beta = 1/\omega_2^2 \qquad \omega_2 = -0.014454 \text{ rad/s} \tag{62}$$

According to the minimum error excitation technique,

$$\boldsymbol{u} = \boldsymbol{M}\boldsymbol{z} \qquad \boldsymbol{M} \triangleq \boldsymbol{F}^*\boldsymbol{C}^\dagger \qquad \boldsymbol{C}^\dagger = \boldsymbol{Q}\boldsymbol{C}^T(\boldsymbol{C}\boldsymbol{Q}\boldsymbol{C}^T)^{-1} \tag{63a}$$

where $\boldsymbol{F}^*$ is a full state feedback controller gain and $\boldsymbol{Q}$ is the variance of the corresponding closed loop state vector $\boldsymbol{x}^*$; that is,

$$\boldsymbol{A}^*\boldsymbol{Q} + \boldsymbol{Q}\boldsymbol{A}^{*T} + \boldsymbol{D}\boldsymbol{V}\boldsymbol{D}^T = 0 \qquad \boldsymbol{A}^* \triangleq \boldsymbol{A} + \boldsymbol{B}\boldsymbol{F}^* \tag{63b}$$

Various closed loop, steady-state performance quantities of interest are

$$\hat{\theta} \triangleq E(\theta_x^2+\theta_y^2)^{1/2}_{\infty} \quad \hat{\dot{\theta}} \triangleq E(\dot{\theta}_x^2+\dot{\theta}_y^2)^{1/2}_{\infty} \quad E(\cdot)_{\infty} \triangleq \lim_{t\to\infty} E(\cdot)$$

$$\hat{E} \triangleq E\Big(\sum_{m\in S} \bar{\alpha}_m \alpha_m\Big)_{\infty} \quad \hat{H} \triangleq E(H_x^2+H_y^2)^{1/2}_{\infty} \quad \hat{u} = E(u_x^2+u_y^2)^{1/2}_{\infty} \tag{64}$$

These will be discussed in Sec. VIII.F for both the approaches OSFB and MEE.

Attention is now drawn to the question of stabilizability of the model (57) with the MEE controller. Note that, due to the absence of any damping, the angular momentum equations (57a) are unstable, but the remaining dynamics is asymptotically stable. Moreover, the variables $H_x(t)$, $H_y(t)$, $\alpha_{mR}(t)$, $\alpha_{mI}(t)$, $m\in S$, are both controllable and observable as manifested by the modal equations (57a) and (57b), the modal expansions of $\theta(t)$ in Eq. (27) and the output equations (45) and (60). This can also be concluded from Theorem 3 of Hughes and Skelton[18] and a theorem by Juang and Balas.[20] Now, a *suitable* feedback controller is required for an arbitrary pole assignment. Wonham[22] has shown that a full state feedback controller is suitable in this sense. On the other hand, Brasch and Pearson[23] have shown that a compensation of order no greater than $\min(\nu_c-1,\nu_0-1)$ is sufficient to assure arbitrary pole placement with output feedback; here $\nu_c(\nu_0)$ is the controllability (observability) index of the plant. For the present spacecraft, it can be shown that $\nu_c-1=\nu_0-1=N$ (the number of modes retained), whereas the output feedback compensation is merely a constant gain controller. It implies that the present suboptimal MEE controller is not capable of assigning the poles arbitrarily. It turns out that the MEE will not be able to stabilize the angular momentum equations, (57a). The optimal state feedback will of course stabilize it.

In Sec. VIII.F we will compare performance of the MEE controller with that of the OSFB. We now raise the final issue: stability of the MEE controller in the presence of modeling uncertainties due to omitted dynamics. This issue is resolved in the next section.

VII. Stability in the Presence of Deleted Modes: A Frequency Domain Approach

Doyle and Stein[24] and Sandell[8] have furnished sufficient conditions of robustness of multivariable feedback systems in the presence of modeling uncertainties. These conditions in the present situation transform to

$$\text{MP:} \quad \bar{\sigma}(\boldsymbol{G}_H\boldsymbol{G}_E^{\dagger}) < \underline{\sigma}[\boldsymbol{I}-(\boldsymbol{G}_E\boldsymbol{G}_a\boldsymbol{M})^{-1}] \qquad \omega>0 \tag{65a}$$

$$\text{AP:} \quad \bar{\sigma}(\boldsymbol{G}_H\boldsymbol{G}_a\boldsymbol{M}) < \underline{\sigma}[\boldsymbol{I}-\boldsymbol{G}_E\boldsymbol{G}_a\boldsymbol{M}] \qquad \omega>0 \tag{65b}$$

where $\underline{\sigma}(\cdot) \triangleq \lambda_{\min}^{1/2}[(\cdot)^*(\cdot)]$ and $\lambda_{\min}(\cdot)$ is the minimum eigenvalue of $(\cdot)$. $\boldsymbol{G}_a$ is the transfer function matrix associated with the two actuators (57d); that is,

$$\boldsymbol{G}_a \triangleq \text{diag}(g_a,g_a) \quad g_a(i\omega) = \omega_a^2/(-\omega^2+2i\zeta_a\omega_a\omega+\omega_a^2) \tag{66}$$

and $(\boldsymbol{I}-\boldsymbol{G}_E\boldsymbol{G}_a\boldsymbol{M})$ is the *return difference matrix* at the output. MP and AP respectively stand for multiplicative and additive perturbation. We did not formulate the additive perturbation in Sec. IV because it required knowledge of the controller gain. Note the presence of $\boldsymbol{M}$ in the left side of Eq. (65b). Also, notice the presence of the multiplicative perturbation $\boldsymbol{L}$ and the singular value $\bar{\sigma}$ in Eq. (65a) as defined in Sec. IV. Since all the deleted modes have nonzero structural damping, the perturbation $\boldsymbol{G}_H$ by itself is stable, and in this theoretical instance it is exact. On the other hand, if the perturbations are unstable, depending on the gains at low frequencies, robustness inequalities may not give reliable results.[25] For two conflicting viewpoints on the utility of singular values and of eigenvalues, Refs. 26 and 27 may be consulted. The above inequalities will be applied to the present gyrostat in Sec. VIII.G.

VIII. Numerical Results and Discussions

The numerical work in this section is performed on the UNIVAC 1110 computer in double precession.

A. Gyroscopic Modes

The rotor's momentum h is the most crucial parameter in the present work. Figure 2 shows dependence of the modal frequencies ω_m and the gyroscopic modes on the h. Figure 2a is constructed by solving the frequency equations (7) by Newton-Raphson technique for the parameters specified in Eq. (1). Figure 2a shows that the stored momentum splits the nongyroscopic frequencies into the two sets defined by Eq. (8). Such a dependence of frequencies on h is well known and is included for completeness (see Hughes and Sharpe[28]). However, note that here the frequencies are obtained by solving two transcendental equations, whereas in the past they were computed from discrete eigenvalue problems. We also observe that for $0\le\bar{h}\le1.0$ the frequency ω_p is close to the first vehicle mode frequency ω_1.

Figure 2b shows variation of $\tilde{G}'_{mLa}$ vs ω_m for various values of $\bar{h}$. We first observe that for $\bar{h}=0.0$ the slope $\tilde{G}'_{mLa}$ varies symmetrically in the positive and the negative range of the frequency. Let us now examine the curves for precessional modes for nonzero $\bar{h}$. We notice that as $\bar{h}$ increases, the $\tilde{G}'_{mLa}$ of a larger and larger number of low-frequency modes reduce. In contrast, however, there exists an intermediate range of frequencies in which $\tilde{G}'_{mLa}$ increases. Moreover, this intermediate range narrows. Beyond this range, $\bar{h}$ has virtually no effect on $\tilde{G}'_{mLa}$. Regarding the antiprecessional modes, the corresponding $\tilde{G}'_{mLa}$ decreases as h increases. These observations signify that, as expected, the rigid body builds resistance to its attitude motion as $\bar{h}$ increases. Some remarks

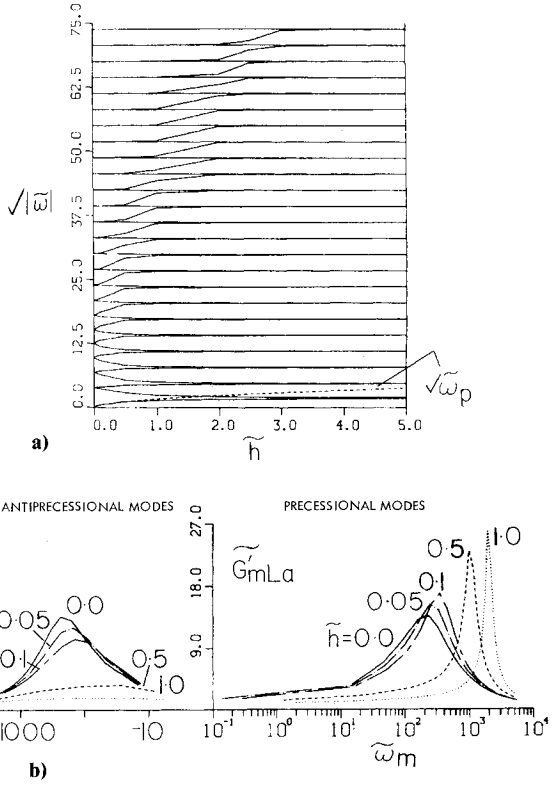

Fig. 2 Modal characteristics of a gyroscopic spacecraft.

on these two types of modes and the associated frequencies are noted in Ref. 29.

B. Modal Identities

Let us verify the momentum identities (9). Define *completeness indexes* $\mathcal{I}_{A1}(N)$ and $I_{A2}(N)$ to repreent the left sides of Eq. (9) such that when $N+\infty$ the two indexes reach their ideal value unity. This terminology is in line with that in Ref. 30 for nongyroscopic spacecraft. Figure 3a shows the growth of $\mathcal{I}_{A1}(N)$ for various values of $\tilde{h}$. When $\tilde{h}$ is relatively small, the first mode is almost like a rigid mode, and, as observed in Fig. 3a, its contribution alone to $\mathcal{I}_{A1}$ is close to unity. As $\tilde{h}$ increases, the dominance of the first mode diminishes and a larger numer of modes is required for $\mathcal{I}_{A1}$ to approach unity. Also, note that the precessional modes add to the index, and the antiprecessional modes subtract. The behavior of the index $\mathcal{I}_{A2}$ is shown in Fig. 3b. The torque T_e is taken to be on the tip of the appendage. Evidently, the approach of $\mathcal{I}_{A2}$ to unity is oscillatory and is less and less convergent as $\tilde{h}$ increases. This is due to the fact that G'_{mLe} evaluated at $z=\ell+a$ is sign-indefinite.

To illustrate the inertial modal identities, let us choose the identity (18), which can be rewritten as

$$\frac{AA_r}{A_e}\sum\frac{G'^2_{mLa}(\omega_m-\omega_p)}{\omega_m}=I \tag{67}$$

Define a *completeness index* $\mathcal{I}_B(N)$ such that it represents the left side of Eq. (67) when ∞ is replaced by N. Figure 4a shows $\mathcal{I}_B(N)$ as N varies from 1 to 48 for various values of $\tilde{h}$. From Fig. 2a it is apparent that, for the range of $\tilde{h}$ considered, the ω_p, at best, is greater than ω_1 and $|\omega_2|$. The remaining $|\omega_m|$'s are always greater than ω_p. Therefore the factor $(\omega_m-\omega_p)/\omega_m$ is always positive for $m\geq 2$. Also, $\mathcal{I}_B(1)$ is generally near zero. Thus we see that $\mathcal{I}_B(N)$ always increases with N, unlike $\mathcal{I}_{A1}(N)$ and $\mathcal{I}_{A2}(N)$. This is confirmed in Fig. 4a. The growth patterns of $\mathcal{I}_B$ in Fig. 4a and the variation of $\mathcal{I}_B(48)$ against h in Fig. 4b become understandable by recalling the dependence of $\bar{G}'_{mLa}$ on $\tilde{h}$ in Fig. 2b. We observe that the growth of $\mathcal{I}_B(N)$ to unity shows as $\tilde{h}$ increases. the other identities can be verified similarly.

Evidently, the indexes $\mathcal{I}_{A1}$, $\mathcal{I}_{A2}$, and $\mathcal{I}_B$ can be used as measures of accuracy of any truncated model. For example, for $\tilde{h}=0.5$ the indexes are

$$\mathcal{I}_{A1}(27)=0.9877 \quad \mathcal{I}_{A2}(27)=0.9729 \quad \mathcal{I}_B(27)=0.9123 \tag{68}$$

as against their ideal value unity. Here N has been chosen such that the oscillations or rapid changes in the indexes have subsided.

Although one infers from Figs. 3 and 4 that a larger number of modes will need to be retained as $\tilde{h}$ increases, we remind ourselves that the identities are only based on inertia and angular momentum of the vehicle and do not consider other important factors such as disturbances, sensed variables, etc. These additional factors necessitate the modal cost analysis which we now exemplify.

C. Modal Cost Analysis

In our numerical work, the highest mode considered will be $m=48$, and the corresponding frequency is $\omega_{48}=-9.48362$ rad/s for $\tilde{h}=0.5$. The limiting number 48 will be justified shortly. As stated in Sec. V, the actuator noise will be ignored and only the exponentially correlated disturbance $\xi_e(t)$ [Eq. (41)] will act on the spacecraft. Let $\tau=0.2$ s, which implies that nearly 70% of the power of the disturbance will be accounted for if we consider frequencies up to 10.0 rad/s. For numerical purposes let the rms value of ξ_e, σ_e, be 0.1 N.m. This fixes V_e in Eq. (41) because $V_e=2\sigma_e^2/\tau$.

Figure 5a shows the modal variances $\hat{\theta}_m$, $\hat{\theta}_{\dot{m}}$, and $\hat{\alpha}_m$ vs ω_m. The variances for the precessional and the antiprecessional modes are drawn separately. It turns out that the three variances for $m=1$ are *far greater* than for $m\geq 2$. This is because the mode $m=1$ is *almost* a rigid mode and must always be retained. Therefore only the variances for $m\geq 2$ are plotted. Further, we note that the variances of any mode outside the range $-10.0\leq\omega\leq 10.0$ is virtually zero. This justifies our confining attention up to $m=48$. Finally, we observe that although $\hat{\theta}_m$ decreases uniformly with ω_m, the variances $\hat{\theta}_{\dot{m}}$ and $\hat{\alpha}_m$ do not. The connotation is that, for the attitude control of the present spacecraft, the modes are important according to frequency, but for attitude rate and "energy" control this is not so. Of course, this inference may change if the parameters in Eq. (1) are changed. The discontinuities in Fig. 5a are due to the discrete nature of ω_m.

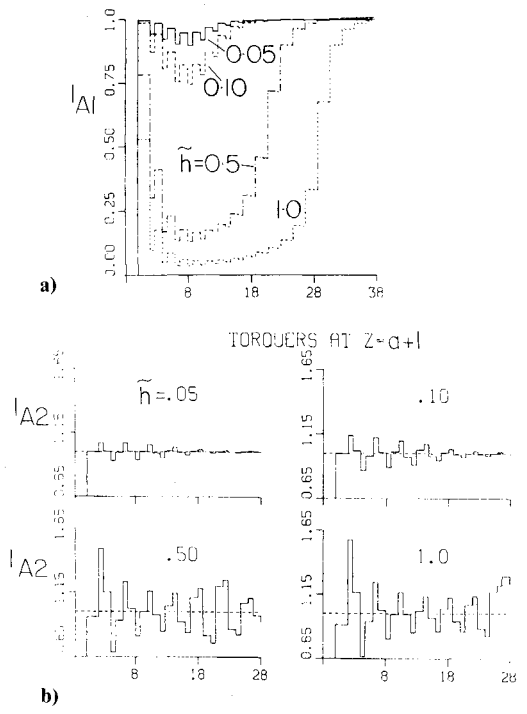

Fig. 3 Verification of angular momentum modal identities.

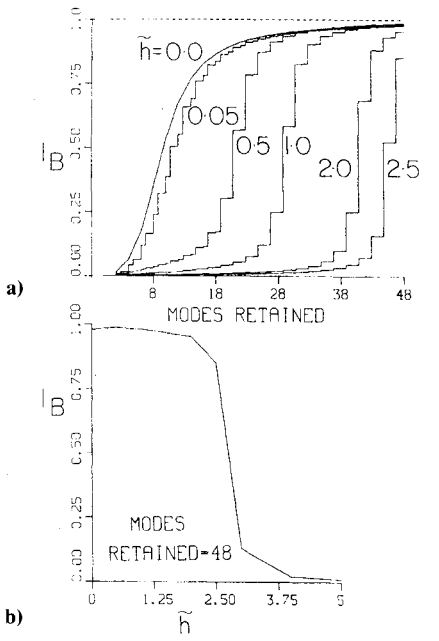

Fig. 4 Verification of inertial modal identities.

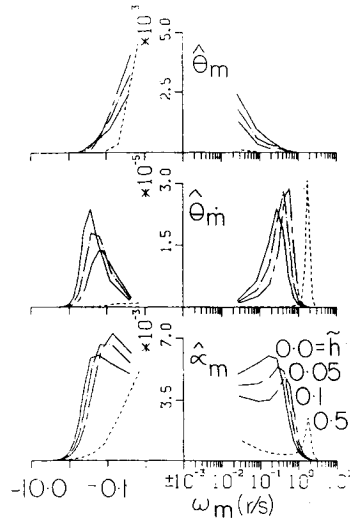

Fig. 5a Modal variances vs frequency.

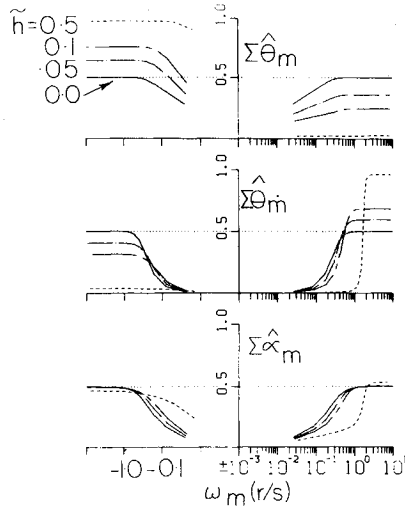

Fig. 5b Cumulative modal variances vs frequency.

Examining the influence of h on the variances, the following facts are discernible. In line with Fig. 2b the variances for $\tilde{h}=0.0$ are symmetric about the $\omega=0.0$ line. This symmetry disappears, as it does in Fig. 2b, as $\tilde{h}$ builds up. The $\hat{\theta}_m$'s for precessional modes decrease and for antiprecessional modes increase as $\tilde{h}$ increases from 0.0 to 0.5. The trends are just the opposite for $\hat{\theta}_{\dot{m}}$. Although $\tilde{h}$ changes the relation between the modal "energy" variance $\hat{\alpha}_m$ and ω_m, $\hat{\alpha}_m$ appears to be well distributed among both the precessional and the antiprecessional modes.

We now examine the variation of the six sums defined as follows

$$\left\{S_{\theta P} \triangleq \sum_{m_{\text{odd}}} \hat{\theta}_m \quad S_{\theta A} \triangleq \sum_{m_{\text{even}}} \hat{\theta}_m\right\}$$

$$\left\{S_{\dot{\theta} P} \triangleq \sum_{m_{\text{odd}}} \hat{\theta}_{\dot{m}} \quad S_{\dot{\theta} A} \triangleq \sum_{m_{\text{even}}} \hat{\theta}_{\dot{m}}\right\} \tag{69}$$

$$\left\{S_{\alpha P} \triangleq \sum_{m_{\text{odd}}} \hat{\alpha}_m \quad S_{\alpha A} \triangleq \sum_{m_{\text{even}}} \hat{\alpha}_m\right\}$$

$$\left\{\sum_{m_{\text{odd}}} \triangleq \sum_{m=3}^{N_P=3,5,\ldots,47} \quad \sum_{m_{\text{even}}} \triangleq \sum_{m=2}^{N_A=2,4,\ldots,48}\right\} \tag{70}$$

For normalization, these three pairs are respectively divided by $\Sigma\{\hat{\theta}_m, \hat{\theta}_{\dot{m}}, \hat{\alpha}_m\}$.

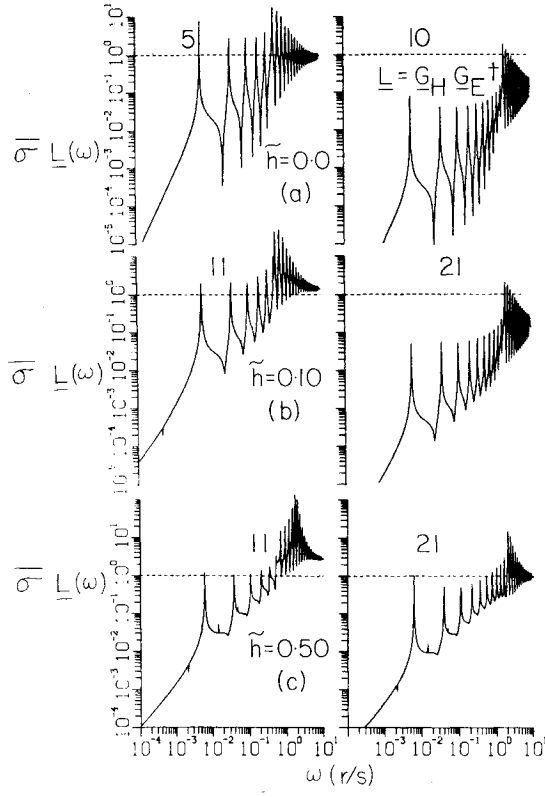

Fig. 6 Truncated modes as a multiplicative perturbation.

The above definitions imply that the maximum value of each sum for $h=0.0$ will be 0.5, as confirmed from Fig. 5b. As $\tilde{h}$ builds up we observe that $S_{\theta P}$ diminishes and $S_{\theta A}$ approaches unity. An opposite trend is noticed in the case of $S_{\dot{\theta} P}$ and $S_{\dot{\theta} A}$. On the other hand, the maximum value of $S_{\alpha P}$ and $S_{\alpha A}$ remains in the neighborhood of 0.5, connoting that the "energy" remains almost equally distributed between the precessional and the antiprecessional modes. The plots such as Fig. 5b systematize the process of finitization of an infinite model from the standpoint of open loop response. Modal cost analysis, however, does not offer any guidance regarding how the deleted modes might affect controller bandwidth in which performance specifications can be met and beyond which stability becomes important. Such clues are obtained next.

D. Deleted Modes as Modeling Uncertainties

Based on the theory in Sec. IV, Fig. 6 displays $\bar{\sigma}(\underline{L})$ for $\tilde{h}=0.0$, 0.1, and 0.5. Here the modes are selected according to frequency. In the next subsection they will be chosen according to modal costs. To meet performance specifications satisfactorily, $\bar{\sigma}(\underline{L})$ should be much less than unity for as wide a range of frequency as possible so that large control gains can be used to compensate for model variations.[24] Figure 6 suggests that this range depends on N and h. In fact, from Fig. 6a for $h=0.0$ and $N=5$ that range is virtually nonexistent. Figure 6a is the plot of $\bar{\sigma}(\underline{L})$ from Eq. (53). The peaks of $\bar{\sigma}$ are zeros of d_E. When N is increased to 10, we see that $\bar{\sigma}(\underline{L})<1$ up to $\omega_{11}=1.9098$ rad/s. In a nongyroscopic situation the dynamics in the two orthogonal planes xz and xy in Fig. 1 is uncoupled. Therefore the N in Fig. 6a represents N elastic modes from each plane. However, when h becomes nonzero, the two uncoupled nongyroscopic modes in two planes transform into a pair of one precessional and one antiprecessional gyroscopic modes (see Fig. 2). Moreover, two uncoupled zero frequency rigid modes coalesce to produce the first gyroscopic mode, $m=1$, which for small h is almost a rigid mode. Consequently, for a proper comparison, the N for Figs. 6b and 6c is twice that of N for Fig. 6a plus 1. From Figs. 6b and 6c, we gather that an increase in N reduces $\bar{\sigma}(\underline{L})$.

but this reduction is impeded as $\tilde{h}$ builds up. The reason is apparent from Fig. 2b. From the numerical results discussed so far, a disadvantage due to h emerges: Other things being equal, a spacecraft with larger momentum requires a larger number of modes for the finite model to have a specified accuracy.

The three criteria, namely, modal identities, modal cost analysis, and deleted modes as modeling uncertainties, will now be fused to create a finite model of the gyrostat in Fig. 1.

E. Finitization of the Model

In the case of nongyroscopic spacecraft, the modal cost analysis is used to establish a sequence of modes according to their contribution to the posed performance objective. The situation, however, is quite complicated in the present gyroscopic case. Here we have two families of modes, precessional and antiprecessional, influenced asymmetrically by the rotor's momentum. The modal identities have somewhat bizarre growth patterns, because contributions from the modes become disproportionate as h increases. Further, the sums $S_{\theta P}$ and $S_{\theta A}$ defined in Eqs. (69) and (70) change antisymmetrically with h; the pair of the sums $S_{\dot{\theta}P}$ and $S_{\dot{\theta}A}$ changes with h in a manner opposite to that of the pair $(S_{\theta P}, S_{\theta A})$. Because of these complications we proceed as follows.

The performance objective is the same as Eq. (61) except that $u_x = u_y = 0$. Therefore the modal cost J_m will be $(\hat{\theta}_m + \beta\hat{\theta}_{\dot{m}})$, where β is given by Eq. (62). For selecting the modes it is expedient to consider $\hat{\theta}_m$ and $\hat{\theta}_{\dot{m}}$ independently and disregard β; a justification for doing so is as follows. Treat the precessional and the antiprecessional modes separately. If we include enough modes from each family such that both the cutoff frequencies are *at least* in the flat portions of the sums in Fig. 5b, then it is inconsequential to consider β. Now, determine the completeness indices $\mathcal{I}_{A1}$ and $\mathcal{I}_B$ for the modes within the two cutoff frequencies. Table 1 is the result of this exercise. Thus, for $\tilde{h} = 0.5$, we retain the following modes.

$$\begin{aligned} &\text{Precessional modes:} && m = 1,3,5,\ldots,23 \\ &\text{Antiprecessional modes:} && m = 2,4,6,8,10 \end{aligned} \tag{71}$$

The resulting finite model is the same as that shown in Sec. V. The modes defined by Eq. (71) are the elements of the set S, Eq. (56). In Table 1, $N_P = 11$ does not include the first precessional mode $m = 1$; this has been added in Eq. (71). Figure 7 shows $\bar{\sigma}(\boldsymbol{L})$, where $\boldsymbol{G}_H$ in $\boldsymbol{L}$ contains the modes beyond those mentioned in Eq. (71) and up to $m = 48$. This should be compared with Fig. 6. It is observed that $\bar{\sigma}(\boldsymbol{L}) < 1$ up to $\omega = 0.5295$ rad/s, which, in fact, is $|\omega_{I2}|$ where $m = 12$ is the ignored mode having lowest absolute frequency. The five indexes, for which ideal values are all unity, in the last row of Table 1 reflect accuracy of the model. Whether this accuracy, and whether the variation of $\bar{\sigma}(\boldsymbol{L})$ vs ω in Fig. 7 are satisfactory will depend on the performance and stability properties of the controller in the presence of the deleted modes. This we will examine in the next two subsections.

F. Performance of the MEE Controller

For computations, the rms value σ_e of the disturbance ξ_e taken to be 0.1 Nm for modal cost analysis is reduced to 0.01 N.m to keep the variables $\theta_x(t)$, $\theta_y(t)$ within the linear range. The actuator parameters are $\omega_a = 10.0$ rad/s and $\zeta_a = 0.7$. The actuator bandwidth should be small so that it may not excite the omitted modes. However, it cannot be arbitrarily small, otherwise the actuator will be ineffective. Indeed, for $\omega_a = 2.0$ rad/s, the actuator was found to be incapable of controlling the model (57) in which the highest frequency is 2.0021 rad/s.

We first compute the optimal state feedback controller gain $\boldsymbol{F}^*$ by solving the usual Riccati equation. For this purpose we employ the subroutine devised by Laub,[31] who uses the Schur vector technique. We next compute the variance $\boldsymbol{Q}$ of the corresponding closed loop state vector by solving the associated Liapunov equation (63b). This is done with the aid of the well-known subroutines ORACLS. The MEE controller gain $\boldsymbol{M}$ can then be calculated by using Eq. (63a). Various performance quantities in Eq. (64) for OSFB and MEE can be "easily" computed by solving corresponding Liapunov equations. Although these quantities are computed on the basis of the retained modes (71), in the interest of economy and on the strength of the five indexes in the last line of Table 1, we believe that they will be close to actual values obtained by retaining all 48 modes *unless* the controller is driven too hard or the system is unstable.

Comparing the performances of the OSFB and the MEE techniques, Fig. 8 shows that both are equally effective in suppressing $\hat{\theta}$ and they both exert equal amounts of control effort $\hat{u}$. As $\hat{u}$ increases, the MEE tends to control the attitude $\hat{\theta}$ and the "energy" $\hat{E}$ as much as the OSFB does. Regarding the angular momentum $\hat{H}$, the OSFB is able to stabilize it by changing the unstable equations (57a) to a stable pair of equations.

$$\dot{H}_x = -H_x/\lambda_x + \xi_x, \qquad \dot{H}_y = -H_y/\lambda_y + \xi_y \tag{72}$$

where, for example, for $\rho = 10$,

$$\tilde{\lambda}_{x,y} = -1.80031 \pm 1.58878 \qquad \lambda_{x,y} = \tilde{\lambda}_{x,y}/\tau_N$$
$$\tau_N = (m_e \ell^3/2EI)^{1/2} \tag{73}$$

These eigenvalues correspond to a damping coefficient $\zeta_H = 2.126310$. Variation of ζ_H, whose minimum value is 1, and of $\hat{H}$ with ρ is shown in Fig. 8. In contrast, as explained in Sec. VI, the MEE controller is not able to stabilize the angular momentum $H(t)$ of the spacecraft. Figure 9 displays the amount of closed loop damping ζ_m introduced by the OSFB and the MEE technique in the modes (71). We learn that while in the low-frequency modes the ζ_m by the OSFB is greater than the ζ_m by the MEE, the consequences are opposite for high-frequency modes.

Thus we conclude that if the sensors are nearly perfect, except for inability to stabilize the angular momentum, the performance of the MEE controller is almost as good as that of an OSFB controller.

Table 1 Completeness indexes of a finite model of the gyroscopic spacecraft in Fig. 1

No. of modes retained	Nature of modes	Highest frequency rad/s	Sum of modal costs for: Attitude θ	Attitude rate, $\dot{\theta}$	"Energy"	$\mathcal{I}A1$	$\mathcal{I}B$
$N_P = 11$	Precessional	2.0021	$S_{\theta P} = 0.0275$	$S_{\dot{\theta}P} = 0.9205$	$S_{\alpha P} = 0.4878$		
$N_A = 5$	Antiprecessional	−0.3580	$S_{\theta A} = 0.9724$	$S_{\dot{\theta}A} = 0.0350$	$S_{\alpha A} = 0.4443$		
16			$S_\theta = 0.999$	$S_{\dot{\theta}} = 0.9555$	$S_\alpha = 0.9321$	0.9687	0.900

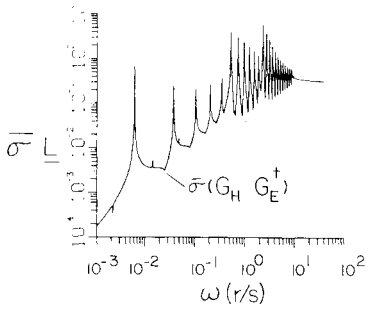

Fig. 7 Truncated modes based on modal cost analysis as a multiplicative perturbation.

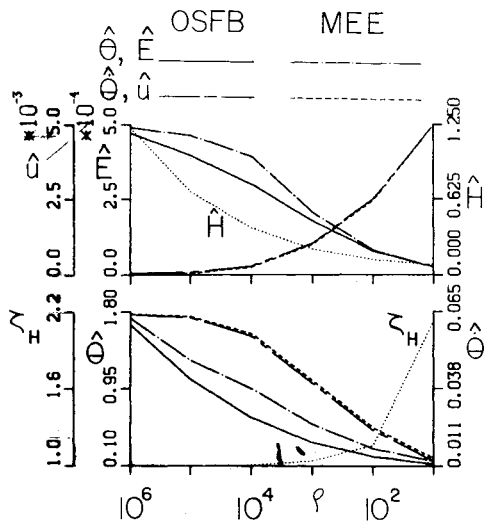

Fig. 8 Performance of optimal state feedback and of minimum error excitation techniques.

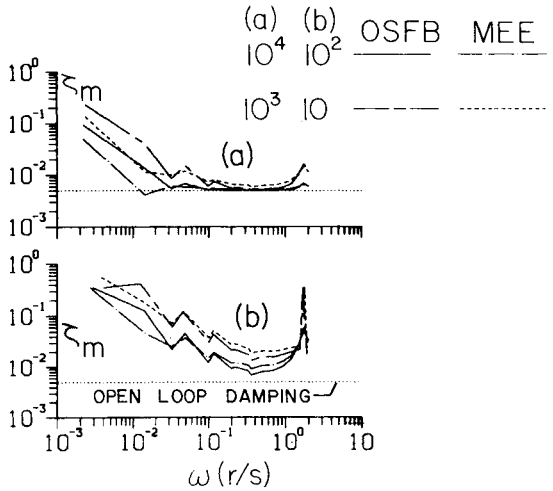

Fig. 9 Closed loop structural damping due to the optimal state feedback and minimum error excitation.

G. Instability Due to Deleted Modes

We will now illustrate the inequalities (65). The complex matrix $G_E G_a M$ tends to be almost singular at high frequencies. Hence the computation of its inverse, appearing in Eq. (65a), leads to unreliable results. Therefore we will illustrate only the additive perturbation inequality. Further, as stated earlier, the MEE approach is unable to stabilize the angular momentum H. This causes numerical difficulties in the computation of the right side of the inequality (65b). To

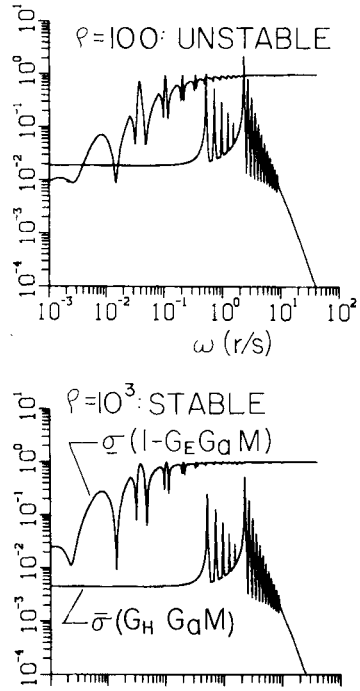

Fig. 10 Influence of deleted modes on stability of the minimum error excitation controller.

redress this situation, we assume that an angular momentum controller has been designed independently of the present study and is given by Eqs. (72) and (73). This replaces the terms $-1/hs$ and $1/hs$ in Eq. (55) by $-1/h(s-\lambda_y)$ and $1/h(s-\lambda_x)$, respectively. The inequality (65b) is illustrated in Fig. 10 after the above modification. We find that for $\rho = 100$, the deleted modes indeed destabilize the system.† The instability is due to the mode $m = 12$, which is the first deleted antiprecessional mode and to the mode $m = 24$, which is next to the mode corresponding to the highest frequency in the retained model. The system is, however, stable for $\rho = 1000$. The corresponding performance of the MEE approach is as follows; the quantities in the bracket correspond to the OSFB approach (see Fig. 8):

$$\hat{\theta}(\text{deg}) = 0.5584\ (0.3573) \qquad \hat{\dot{\theta}}(\text{deg/s}) = 0.04092\ (0.03994)$$

$$\hat{E}(\text{N.m}) = 2.0503 \times 10^{-4}\ (1.7677 \times 10^{-4})$$

$$\hat{u}(\text{N.m}) = 0.000984\ (0.001021)$$

Acceptability of this performance will depend on specifications.

IX. Closing Comments

A thorough investigation of the dynamics of a gyroscopic spacecraft and a synthesis of its controller are performed in the preceding. Although the findings, summarized below, are derived from the response of a specific deformable gyrostat, they seem to be typical. Our findings are

1) The infinite number of gyroscopic modes have, alternately, a precession parallel and antiparallel to the rotor's

†We were late in realizing that the conditions (65) are sufficient but not necessary for stability. Ref. 11 shows that although the inequalitites (65) predict instability for a certain scalar controller gain for a simple free beam, the eigenvalue analysis did *not* detect any instability even when the gain was increased by a factor of 8.5. When the factor was g, the instability was found. This leads us to believe that the instability shown in Fig. 10 does not actually exist. We wish to seek an aplogy for this oversight.

momentum h. The slope of the modes at the rotor's location exhibits a complicated relationship with h.

2) The formulation of gyroscopic modes systematize the study of random vibrations of a gyroscopic spacecraft subject to arbitrary excitation. Such a study facilitates a modal cost analysis.

3) Modal identities and modal cost analysis involving the rotor's momentum furnish useful metrics to assess the accuracy of the finitized models of a deformable gyrostat.

4) With the escalation of the rotor's momentum, a larger number of modes will be required to construct a finite model of prespecified accuracy.

5) Omitted high-frequency modes can be modeled as a multiplicative or an additive perturbation in an idealized transfer function. Singular values of the perturbation matrix provide a norm to determine the bandwidth of a multivariable controller. This bandwidth depends on retained modes and the rotor's momentum.

6) In the absence of sensor noise, the minimum error excitation (MEE) approach (a suboptimal output feedback scheme) is almost as effective as an optimal state feedback (OSFB). However, if attitude and rate sensors only are used, the MEE cannot stabilize the vehicle's angular momentum.

7) The damping induced in low-frequency modes by the MEE is smaller than that by the OSFB. Opposite effects are observed in the case of high-frequency modes.

We believe that the efforts reported here provide valuable insight into the natural as well as controlled behavior of gyroscopic spacecraft.

Acknowledgments

We acknowledge the perceptive discussions and encouragement of Dr. R.C. Ried, Head of Aerothermodynamics Section, NASA Johnson Space Center, Houston, at various stages of our endeavors. We are indebted to the National Research Council for financial support. We are thankful to Dr. C.D. Scott who read and commented on the draft. With much pleasure, we also thank the reviewers for their critical reviews.

References

[1] Meirovitch, L., "A Modal Analysis of the Response of Linear Gyroscopic Systems," *Journal of Applied Mechanics,* Vol. 42, June 1975, pp. 446-450.

[2] Oz, H. and Meirovitch, L., "Optimal Modal Space Control of Flexible Gyroscopic Systems," *Journal of Guidance and Control,* Vol. 3, May-June 1980, pp. 218-226.

[3] Skelton, R., "Adaptive Orthogonal Filters for Compensation of Modal Errors in Matrix-Second-Order Systems," *Journal of Guidance and Control,* Vol. 4, March-April 1981, pp. 214-221.

[4] Skelton, R.E., "Cost Decomposition of Linear Systems with Application to Model Reduction," *International Journal of Control,* Vol. 32, June 1980, pp. 1031-1055.

[5] Sezer, M.E. and Siljak, D.D., "Validation of Reduced Order Models for Control Systems Design," *Journal of Guidance, Control, and Dynamics,* Vol. 5, No. 5, Sept.-Oct. 1982, pp. 430-437.

[6] Hablani, H.B., "Modal Analysis of Gyroscopic Flexible Spacecraft: A Continuum Approach," *Journal of Guidance, Control, and Dynamics,* Vol. 5, Sept.-Oct. 1982, pp. 448-457.

[7] Kosut, R.L., "Suboptimal Control of Linear Time Invariant Systems Subject to Control Structure Constraints," *IEEE Transactions on Automatic Control,* Vol. AC-15, Oct. 1970, pp. 557-563.

[8] Sandell, N.R., "Robust Stability of Multivariable Feedback Systems," *16th Annual Allerton Conference on Communication, Control, and Computing,* Monticello, Ill., Oct. 1978, pp. 471-479.

[9] Hughes, PC., "Modal Identities for Elastic Bodies, with Application to Vehicle Dynamics and Control," *Journal of Applied Mechanics,* Vol. 47, March 1980, pp. 177-184.

[10] Skelton, R.E. and Hughes, P.C., "Modal Cost Analysis for Linear Matrix-Second-Order Systems," *Journal of Dynamic Systems, Measurement, and Control,* Vol. 102, Sept. 1980, pp. 151-158.

[11] Hablani, H.B., "Stochastic Response Analysis, Order Reduction, and Output Feedback Controllers for Space Structures," *Journal of Guidance, Control, and Dynamics.* (Under review).

[12] Elishakoff, I., Van Zanten, A.T., and Crandall, S.H., "Wide-Band Random Axisymmetric Vibration of Cylindrical Shells," *Journal of Applied Mechanics,* Vol. 46, June 1979, pp. 417-422.

[13] Hughes, P.C., "Modal Cost Analysis as an Aid in Control System Design for Large Space Structures," *NCKU/AAS Symposium on Engineering Science and Mechanics,* Tainan, Taiwan, Dec. 1981.

[14] Skelton, R.E., "Control Design of Flexible Spacecraft," AGARDOGRAPH No. 251, Theory and Application of Optimal Control in Aerospace Systems, edited by P. Kant, NASA Langley Field, Va., Chap. 8.

[15] Kwakernaak, H. and Sivan, R., *Linear Optimal Control Systems,* Wiley Interscience, New York, 1972.

[16] Hildebrand, F.B., *Advanced Calculus for Applications,* 2nd ed., Prentice Hall, Englewood Cliffs, N.J., 1976, Chap. 10, pp. 539-621.

[17] Moore, B.C., "Principal Component Analysis in Linear Systems: Controllability, Observability, and Model Reduction," *IEEE Transactions on Automatic Control,* Vol. AC-26, No. 1, Feb. 1981, pp. 17-32.

[18] Hughes, P.C. and Skelton, R.E., "Controllability and Observability of Linear Matrix-Second-Order Systems," *Journal of Applied Mechanics,* Vol. 47, June 1980, pp. 415-420.

[19] Likins, P.W. and Ohkami, Y., "Coordinate Transformation and Truncation for Rotating Spacecraft with Flexible Appendages," *AIAA Journal,* Vol. 13, Dec. 1975, pp. 1657-1665.

[20] Juang, J.N. and Balas, M., "Dynamics and Control of Large Spinning Spacecraft," *Journal of the Astronautical Sciences,* Vol. 28, Jan.-March 1980, pp. 31-48.

[21] Ashkenazi, A. and Bryson, A.E., "The Synthesis of Control Logic for Parameter-Insensitivity and Disturbance Attenuation," *Proceedings of AIAA Guidance and Control Conference,* Danvers, Mass., Aug. 1980, pp. 11-17.

[22] Wonham, W.H., "On the Pole Assignment in Multi-Input Controllable Linear Systems," *IEEE Transactions on Automatic Control,* Vol. AC-12, Dec. 1967, pp. 660-665.

[23] Brasch, F.M. and Pearson, J.B., "Pole Placement Using Dynamic Compensators," *IEEE Transactions on Automatic Control,* Vol. AC-15, Feb. 1970, pp. 34-43.

[24] Doyle, J.C. and Stein, G., "Multivariable Feedback Design: Concepts for a Classical/Modern Synthesis," *IEEE Transactions on Automatic Control,* Vol. AC-26, Feb. 1981, pp. 4-16.

[25] Stein, G. and Doyle, J.C., "Singular Values and Feedback: Design Examples," *16th Annual Allerton Conference on Communication, Control, and Computing,* Monticello, Ill., Oct. 1978, pp. 461-470.

[26] Mukhopadhyay, V. and Newsom, J.R., "Application of Matrix Singular Value Properties for Evaluating Gain and Phase Margins of Multiloop Systems," *Proceedings of AIAA Guidance and Control Conference,* San Diego, Calif., Aug. 1982, pp. 420-428.

[27] Doyle, J.C., "Robustness of Multiloop Linear Feedback Systems," *Proceedings of the 1978 IEEE Conference on Decision and Control,* San Diego, Calif., Jan. 1979, pp. 12-18.

[28] Hughes, P.C. and Sharpe, H.N., "Influence of Stored Angular Momentum on the Modal Characteristics of Spacecraft with Flexible Appendages," *Journal of Applied Mechanics,* Vol. 42, Dec. 1975, pp. 785-788.

[29] Skelton, R.E., Hughes, P.C., and Yang, H.T., "Dynamics and Control of Flexible Spacecraft," *Fourth AIAA/UCLA Continuing Education Lecture Series,* Lecture Notes, June 1981, Chap. 5.

[30] Hughes, P.C. and Skelton, R.E., "Modal Truncation for Flexible Spacecraft," *Journal of Guidance and Control,* Vol. 4, May-June 1981, pp. 291-297.

[31] Laub, A., *A Schur Method for Solving Algebraic Riccati Equations,* Massachusetts Institute of Technology, Cambridge, Mass. LIDS-R-859, Oct. 1978.